BRIEF COMMUNICATION

AMERICAN JOURNAL OF
BIOLOGICAL ANTHROPOLOGY
The Official Journal of the American Association of Biological Anthropologists

WILEY

Homo naledi lumbar vertebrae and a new 3D method to quantify vertebral wedging

Scott A. Williams [1,2,3,4] | Iris Zeng [5] | Jordan S. Guerra [1,2] | Shahed Nalla [3,6] |
Marina C. Elliott [3,7] | John Hawks [3,8] | Lee R. Berger [3] | Marc R. Meyer [9]

[1]Center for the Study of Human Origins, Department of Anthropology, New York University, New York, New York, USA

[2]New York Consortium in Evolutionary Primatology, New York, New York, USA

[3]Centre for the Exploration of the Deep Human Journey, University of the Witwatersrand, Johannesburg, South Africa

[4]Evolutionary Studies Institute, University of the Witwatersrand, Johannesburg, South Africa

[5]Department of Architecture, Massachusetts Institute of Technology, Cambridge, Massachusetts, USA

[6]Department of Human Anatomy and Physiology, Faculty of Health Sciences, University of Johannesburg, Johannesburg, South Africa

[7]Department of Archaeology, Simon Fraser University, Burnaby, British Columbia, Canada

[8]Department of Anthropology, University of Wisconsin, Madison, Wisconsin, USA

[9]Department of Anthropology, Chaffey College, Rancho Cucamonga, California, USA

Correspondence
Scott A. Williams, 25 Waverly Place, New York, NY 10003, USA.
Email: sawilliams@nyu.edu

Funding information
Leakey Foundation

Abstract

Objectives: In humans and known fossil hominins, lumbar lordosis is produced by vertebral body wedging and other bony and soft tissue features such as the shape of the intervertebral discs. Current techniques for quantifying the wedging of vertebral bodies are limited in utility, especially when analyzing incomplete fossil material. Here, we introduce a 3D method to quantify vertebral body wedging angles that yields the angles between two "best fit" planes in the software GeoMagic Wrap (3D Systems).

Materials and Methods: To test that this new method is repeatable with existing methods, we measure the wedging of 320 lumbar vertebrae representing 64 modern human individuals. For each vertebra, wedging angles were calculated from linear measurements taken with calipers and compared with estimates generated from the 3D best fit plane method. We also apply the 3D plane method to fossil hominin lumbar vertebrae, including newly described lumbar vertebrae of *Homo naledi*, the majority of which do not preserve the four landmarks necessary to calculate wedging angles using the traditional approach.

Results: The results of the two methods are highly and significantly correlated ($r^2 = 0.98$, $p < 0.0001$). The 3D plane method was successfully applied to nearly all of the fossil hominin specimens included in the study.

Discussion: The new 3D plane method introduced here is repeatable with the traditional linear measurement method and allows for the estimation of wedging angles in incomplete material. When applied to *Homo naledi* lumbar vertebrae, similarities to other fossil hominins and modern humans are found.

KEYWORDS
Australopithecus, bipedalism, *Homo*, lordosis, posture

1 | INTRODUCTION

Hominins evolved lumbar lordosis, or dorsal concavity of the lower lumbar column, as an adaptation to bipedalism at some point relatively early in their evolutionary history (Been et al., 2012; Latimer & Ward, 1993; Whitcome et al., 2007; Williams et al., 2013; Williams et al., 2021). Lumbar lordosis allows an upright biped to efficiently balance the upper body over the hip joints and lower limbs. Clinical studies on modern human spinal curvature are abundant, and several techniques for quantifying lordosis on lateral radiographs have been formalized (reviewed in Been & Kalichman, 2014). However, the fragmentary nature of the hominin fossil and archeological records does not allow the direct application of these methods. Frequently, processes (articular, transverse, and spinous) are not fully preserved, nor

are vertebral bodies. The traditional approach to osteological and fossil material (but see Zlolinski et al., 2019 for a 3D Geometric Morphometric approach) has been to take three measurements of a vertebral body (ventral body craniocaudal height, dorsal body craniocaudal height, and superior body dorsoventral length) by either placing 3D landmarks or sliding calipers on four landmarks (ventral-most point on the superior vertebral body at midline, ventral-most point on the inferior vertebral body at midline, dorsal-most point on the superior vertebral body at midline, and dorsal-most point on the inferior vertebral body at midline). Those data are then used to calculate a wedging angle (DiGiovanni et al., 1989). This method is not applicable if the vertebral body is damaged at, or otherwise missing, any of the four landmarks. These measurements can be approximated with calipers using more lateral aspects of the ventral or dorsal vertebral body, but this correction adds potential error to a sensitive equation. Alternatively, lateral photographs of individual vertebrae can be taken (akin to lateral radiographs), then 2D planes can be fit to the superior and inferior vertebral body surfaces and their angle measured. This approach is sensitive to the orientation of the vertebra relative to the camera lens and uses the lateral aspects of the vertebral body rather than its midline to estimate wedging angles. Here, we employ a 3D plane approach to quantify vertebral wedging angle and infer lumbar lordosis in a fossil hominin with fragmented vertebral bodies, *Homo naledi*.

Homo naledi is currently known from a large number of individuals from the Dinaledi Chamber (U.W. 101) (Berger et al., 2015; Williams et al., 2017) and at least two partial skeletons from the Lesedi Chamber (U.W. 102a), including an adult male (Hawks et al., 2017). This individual, LES1, preserves a partial vertebral column, including three lower thoracic vertebrae and four lumbar vertebrae (Hawks et al., 2017). The lumbar vertebrae are seriated based on their relationships to one another, to the last thoracic vertebra (U.W. 102a-154A) and to a newly recovered sacrum (U.W. 102-596). One element (the third lumbar vertebra) has not been recovered. The first, second and penultimate lumbar vertebrae preserve vertebral bodies but significant aspects of their neural arches are absent, whereas the last lumbar vertebra preserves a partial neural arch in addition to a broken vertebral body. Here we describe the lumbar vertebrae along with a new sacral element recovered elsewhere in the Lesedi Chamber (Figure 1). We quantify vertebral wedging in the U.W. 102a material using our proposed 3D plane technique and compare these data to other fossil hominins and a global archeological sample of modern humans.

2 | MATERIALS AND METHODS

We created surface scans of complete lumbar columns of 64 adult modern humans (32 females and 32 males), totaling 320 vertebrae. Individuals demonstrating obvious pathologies, especially those affecting the bilateral symmetry of vertebral bodies (e.g., scoliosis), were not included. Postindustrial peoples possess more exaggerated lumbar lordosis than preindustrial, "traditional-living" peoples (Williams et al., 2022), so the sample used here is a global archeological
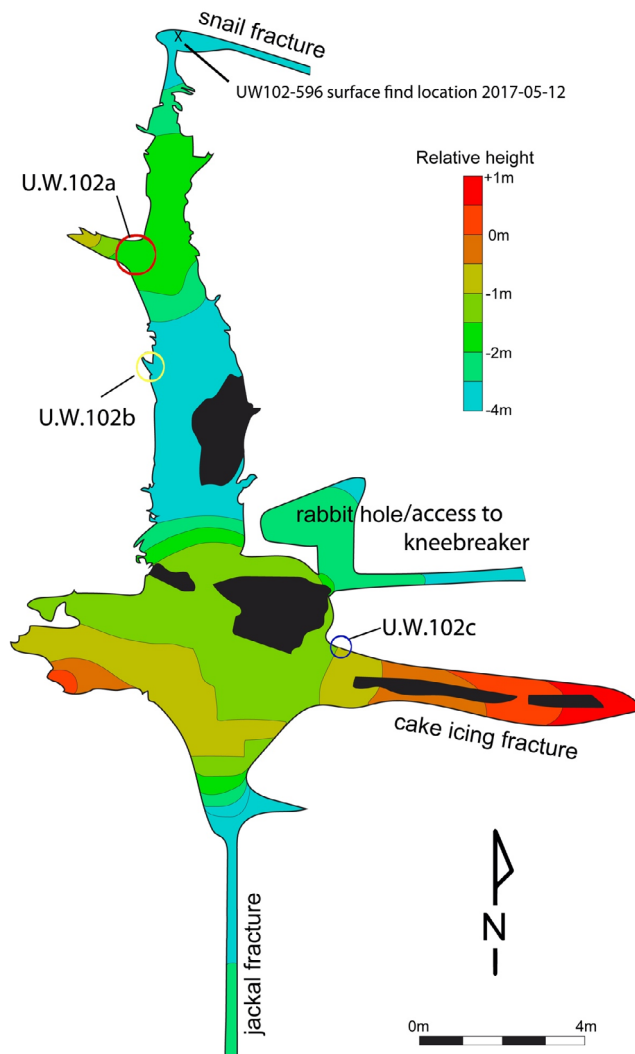

FIGURE 1 Schematic of the Lesedi Chamber of Rising Star Cave. The partial skeleton LES1 was recovered from the U.W. 102a location. The new partial sacrum, U.W. 102-596, is a surface find from the "snail fracture" located approximately 5 m north of U.W. 102a

sample (with specimens from southern, eastern, and northern Africa, South and East Asia, Northern Europe, Polynesia, Australia, and the Americas). Additionally, we created surface scans of the *H. naledi* lumbar vertebrae (U.W. 102a-154B, U.W. 102a-322, U.W. 102a-306, and U.W. 102a-139), as well as those of other available fossil hominins: Kebara 2 and Shanidar 3 (Neandertals), Sts 14a-f, StW 431, StW 572, StW 656, and StW 600 (*A. africanus*) (Pickering et al., 2019), U.W. 88-232-234/153, U.W. 88-126/138 (*A. sediba*) (Williams et al., 2021), SK 3981b (*Paranthropus robustus* or early *Homo*), A.L. 288-1aa, A.L. 333-7, and A.L. 444-7 (*A. afarensis*) (Ward et al., 2012). Original fossil specimens were scanned in all cases except the Neandertals, where high-quality casts were studied. In the case of Sts 14, reconstructed aspects of the vertebrae were ignored, following Ward and colleagues (Ward et al., 2020).

Three-dimensional (3D) models of each vertebra were created using an Artec Space Spider scanner and Artec Studio software
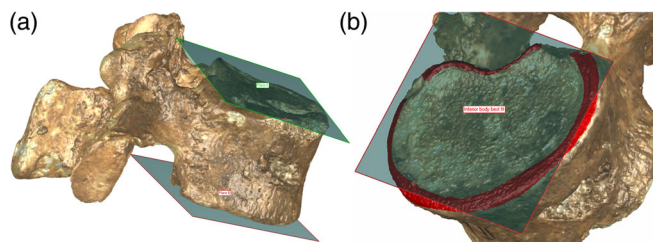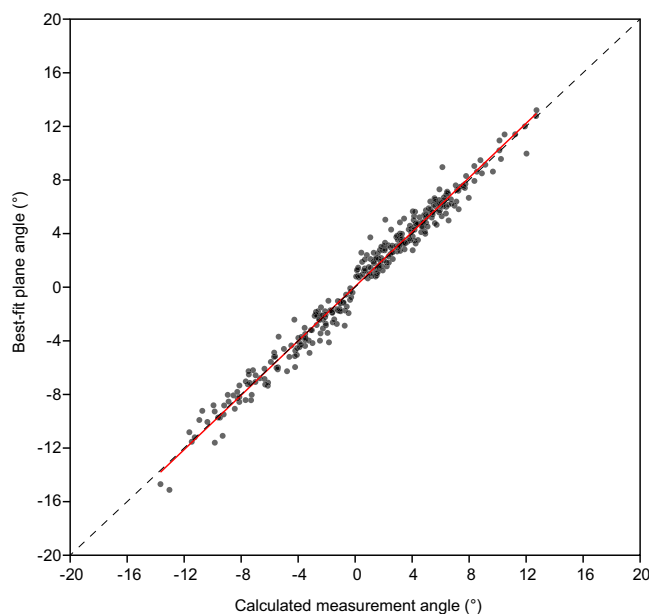
FIGURE 2 The best-fit plane method of vertebral body wedging angle estimation demonstrated using GeoMagic Wrap (3D Systems). (a) Best-fit planes fitted to the superior vertebral body (top; green) and inferior vertebral body (bottom; red). (b) Planes are fitted by highlighting (in red) aspects of the vertebral body that capture its orientation, in this case the preserved aspects of the annular apophysis
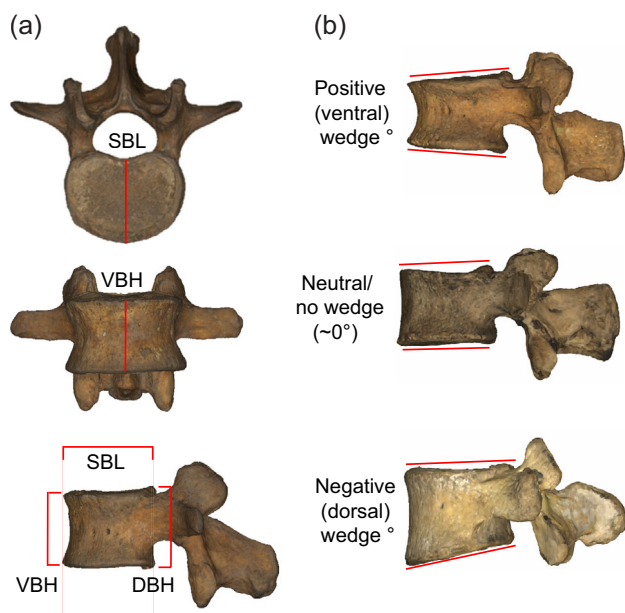
FIGURE 3 Measurements of the vertebral body to derive the wedging angle. (a) Linear measurements required to calculate wedging angle (SBL = superior body dorsoventral length, M4; DBH = dorsal body craniocaudal height, M2; VBH = ventral body craniocaudal height, M1). (b) Directly measured wedging angle that is estimated using the wedging angle equation and is similar to the best-fit plane angle method. As opposed to the vertebra in (b), which demonstrates strong ventral wedging, (c) shows relatively neutral wedging (left) and strong dorsal wedging (right)

FIGURE 4 Regression of the best-fit plane angle method results and those of the linear measurement calculated angle method on the same set of 320 lumbar vertebrae ($N = 64$ individuals). The ordinary least squares regression line ($y = 0.057 + 1.01 * X$) is shown in red and is nearly identical to the $X = Y$ (dashed) line; other lines (e.g., reduced major axis) are extremely similar as expected with a high correlation coefficient (Smith, 1984). The correlation is high and significant ($r^2 = 0.978$; $p < 0.0001$). Data points are set to 60% opacity, so darker shades represent high density of points in the same area

(Artec 3D, Luxembourg). Polygon (PLY) files were exported and loaded in GeoMagic Wrap software (3D Systems, Rock Hill, SC). In Wrap, surfaces of the superior and inferior vertebral bodies reflecting their contours were highlighted and best-fit planes (Features → Planes → Best Fit) were fit to each, using the Contact Surface option (Figure 2). The best-fit planes are examined to check that the planes are parallel to one another in dorsal or ventral view (i.e., not asymmetrical in orientation). The 3D models were then rotated to lateral view to ensure that both planes adequately quantify the angle of the vertebral body surfaces. Note that the planes themselves cannot be manipulated; rather, surface highlighting can be manipulated if the plane does not appear to correspond well to the vertebral body surface. For example, in some instances, the lateral aspects of the inferior surface of the vertebral body are highly concave and/or asymmetrical and cause the best-fit plane to not conform to the dorsal and ventral aspects of the inferior vertebral body; in these instances, highlighting can be removed from those aspects of the vertebra so that the plane better reflects the orientation of the surface. We then calculate the angle between the two best-fit planes (Measure → Angle).

Digital calipers were used to collect the three measurements necessary to calculate vertebral body wedging: superior vertebral body dorsoventral length at midline (SBL, Martin measurement #4 [M4]) (Bräuer, 1988), dorsal vertebral body craniocaudal height at midline (DBH; M2), and ventral vertebral body craniocaudal height at midline (VBH; M1) (Figure 3). These three measurements were used to calculate the wedging angle (DiGiovanni et al., 1989):

$$\arctan\left(\left(\left(\left(DBH - VBH\right)/2\right)/SBL\right) * 2\right)$$

This calculated wedging angle was then compared to the 3D plane method using a paired t-test across all vertebrae and in a linear regression in PAleontological STatistics (PAST) version 2 (Hammer et al., 2001). In both cases, we use an alpha level of 0.05 for statistical significance.

Group	L1	L2	L3	L4	L5
Human ♂	6.5 (2.5)[a]	5.7 (2.8)	4.1 (3.2)	0.3 (3.0)	−6.5 (2.4)
Human ♀	4.7 (2.2)	2.7 (2.6)	0.0 (3.2)	−2.6 (2.7)	−7.1 (3.8)
LES1	3.7	2.9	-	2.4	−4.8
Kebara 2	5.2	9.1	9.4	4.1	−12.4
Shanidar 3	8.3	8.5	5.6	−0.7	−7.9
MH2	-	4.9	1.3	−2.5	−11.7
Sts 14	2.7	2.3	2.2	−3.0	−4.8
StW 431	5.9	2.0	3.9	1.2	−3.8
Other StW[b]	-	6.2	6.8	-	−4.1
SK and A.L.[c]	-	-	2.0/7.1	-	−3.7

TABLE 1 Best-fit 3D wedging angle data on male and female humans and fossil hominin specimens

[a]Means and standard deviations (parentheses) are included for the modern human sample.
[b]StW 572 (L2), StW 656 (L3), and StW 600 (L5).
[c]A.L. 288-1 (L3, right), A.L. 333-73 (L3, left), and SK 3981b (L5).
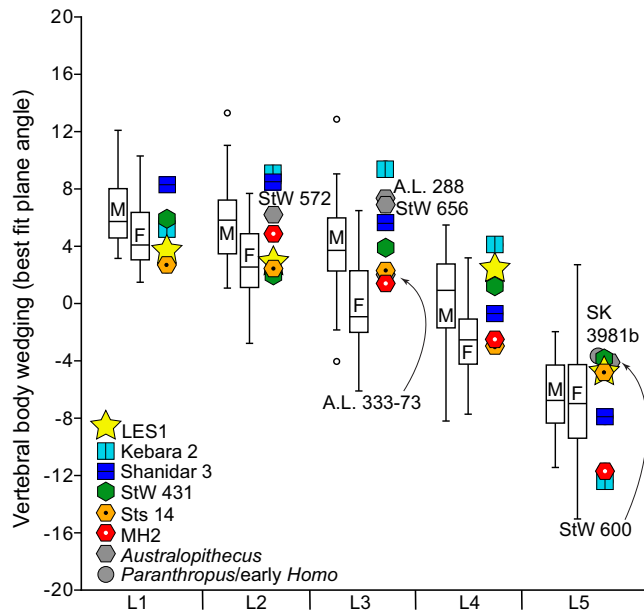
FIGURE 5 Best-fit plane wedging angles presented at each lumbar level. Modern human males (M) and females (F) are significantly different at each level ($p < 0.05$) except the last lumbar level ($p = 0.48$). Fossil hominins are shown at each lumbar level; those represented by more than one fossil are identified in the key (LES1 = presumed male *H. naledi* from the Lesedi Chamber; Kebara 2 and Shanidar 3 = male Neandertals from the Levant; StW 431 and Sts 14 = male and female, respectively, of *A. africanus* from Sterkfontein; MH2 = female *A. sediba* from Malapa), whereas those represented only once are labeled directly in the graph (StW 572, StW 656, and StW 600 = *A. africanus* individuals from Sterkfontein; a.L. 288 and a.L. 333-71 = female and unknown sex, respectively, of *A. afarensis* from Hadar; SK 3981b = unknown affinity, but possibly *P. robustus* or early *Homo*, from Swartkrans). Outliers in the modern human sample are shown as open circles and do not represent extreme outliers
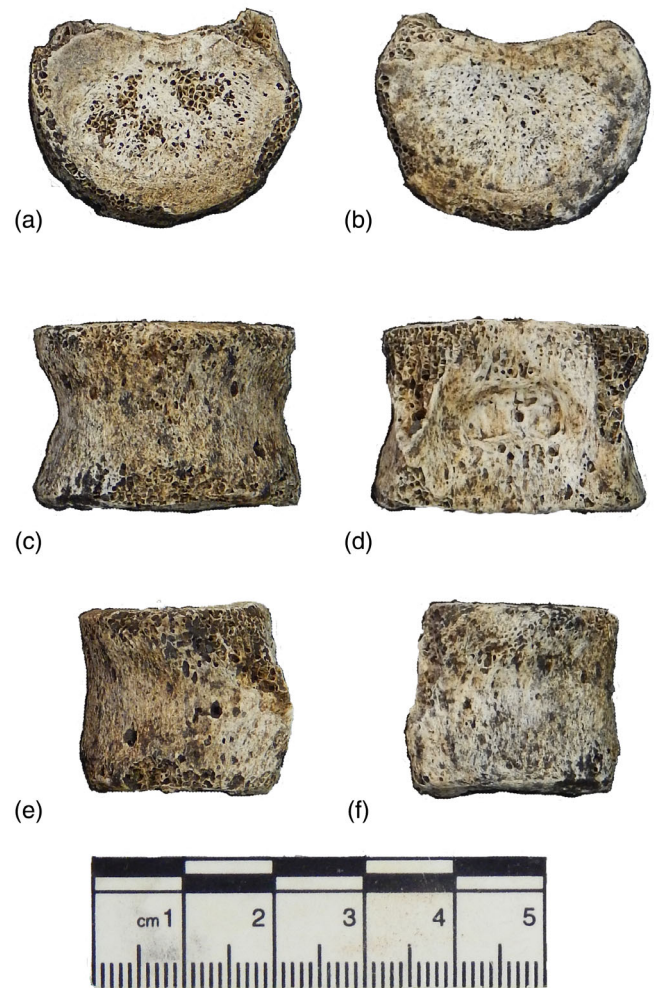
FIGURE 6 First lumbar vertebra (L1), U.W. 102a-154B. Views are (a) cranial, (b) caudal, (c) ventral, (d) dorsal, (e) left lateral, and (f) right lateral

TABLE 2 Preserved standard measurements of the LES1 lumbar vertebrae

| Measurements (in mm)	U.W. 102a-154B (L1)	U.W. 102a-322 (L2)	U.W. 102a-306 (L4)	U.W. 102a-139 (L5)
VBH (M1)	20.8	20.2	-	-
DBH (M2)	22.2	21.3	19.1	-
SBW (M7)	30.3		-	-
BSL (M4)	20.4	-	-	-
IBW (M5)	-	-	-	32.5
IBL (M8)	-	22.0	-	-

3 | RESULTS

3.1 | Comparison of linear and 3D wedging angle estimates

The results of the two wedging angle estimation methods are not significantly different from each other (paired t-test: $t = -1.502$, $p = 0.134$). We found a high, significant correlation ($r^2 = 0.978$, $p < 0.0001$), suggesting the two measurements are quantifying similar aspects of morphology (Figure 4). The human male and female and fossil hominin best-fit angle results are presented in Table 1.

We describe the *H. naledi* lumbar vertebrae and sacrum from the Lesedi Chamber of Rising Star Cave (Hawks et al., 2017) below. Only the first lumbar vertebra preserves the adequate midline landmarks to take vertebral body measurements and calculate the wedging angle. We also estimate a 3D wedging angle for L1 and the remaining lumbar vertebrae. We include them and other fossil lumbar vertebrae in level by level plots of 3D best-fit plane wedging estimates (Figure 5).

3.2 | First lumbar vertebra

U.W. 102a-154B is the body of a first lumbar vertebra (L1) (Figure 6). Its position in the vertebral column is determined both serially and anatomically—it follows the last thoracic vertebra, U.W. 102a-154A, determined due to its position relative to the three lower thoracic vertebrae that precede it (cranially-caudally: U.W. 102a-036, U.W. 102a-151, 102a-154A; described in Hawks et al., 2017) and the presence of costal facets. U.W. 102a-154B preserves no evidence of costal facets, and is missing all but small inferior portions of the pedicles. The left side is somewhat better preserved in this regard, and cross-sections of the pedicles are visible at their roots on the vertebral body. They extend approximately 2/3 of the craniocaudal height of the vertebral body from its superior aspect and taper mediolaterally, forming a V-shape caudally. The superior surface of the vertebral body is mostly preserved, with some chipping of the annular apophysis, particularly on the dorsal and left lateral side. The center of the superior surface is abraded, exposing small areas of trabeculae. The inferior vertebral body surface is smooth at its center, with the annular apophysis present but is damaged dorsally and on the left lateral side. Many of the vertebral body measurements of U.W. 102a-154B can be directly measured using digital calipers and are reported in Table 2. The
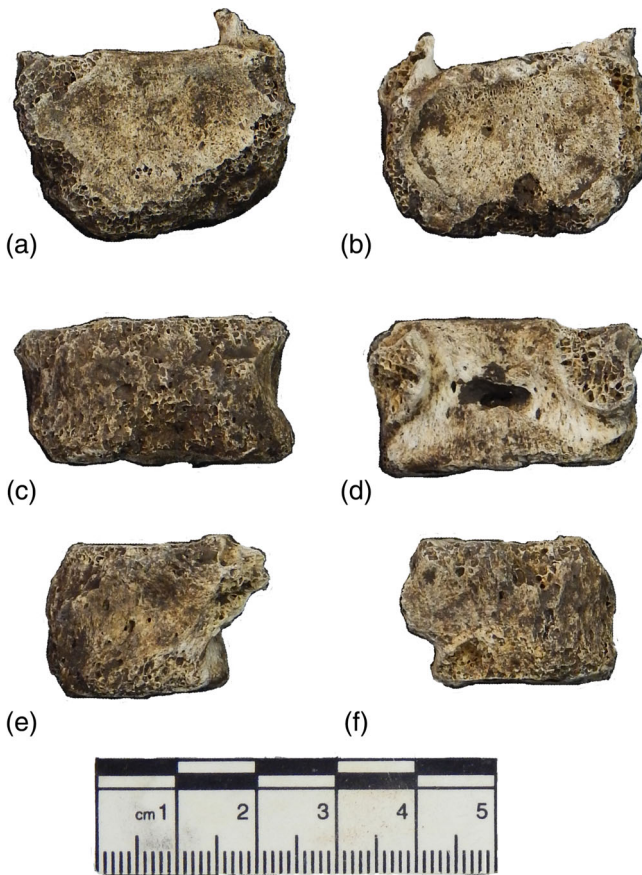

(a)   (b)

(c)   (d)

(e)   (f)
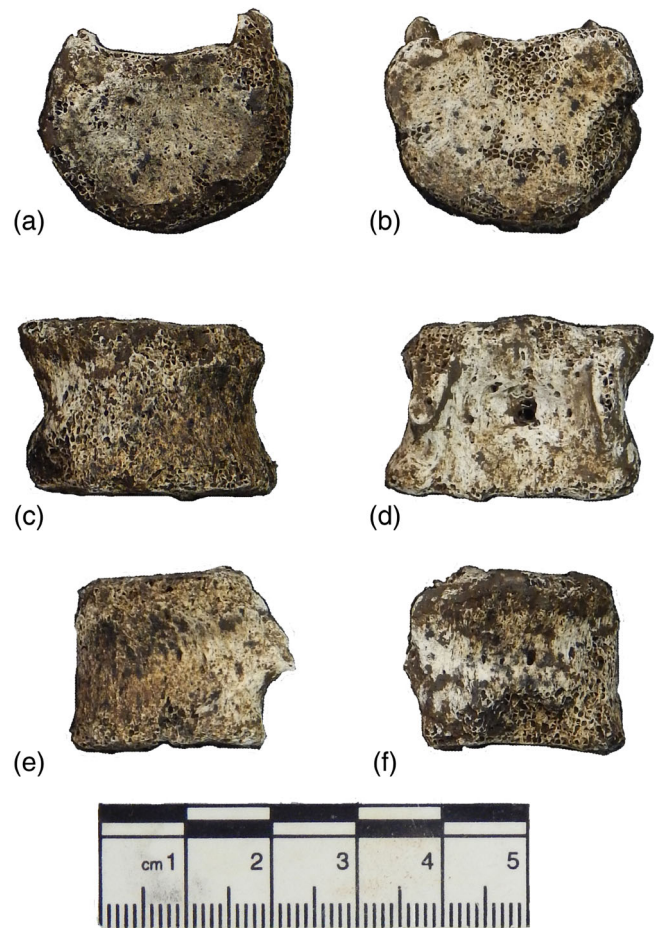
FIGURE 7 Second lumbar vertebra (L2), U.W. 102a-322. Views are (a) cranial, (b) caudal, (c) ventral, (d) dorsal, (e) left lateral, and (f) right lateral

estimated 3D wedging angle is 3.7°, which is very similar to the calculated wedging angle of 3.8°.

3.3 | Second lumbar vertebra

U.W. 102a-322 is the body as a second lumbar vertebra (L2) (Figure 7). Portions of the bases of the left and right pedicles are present, with the preserved aspect of the left pedicle projecting more dorsally than the right. The vertebral body bears a basivertebral
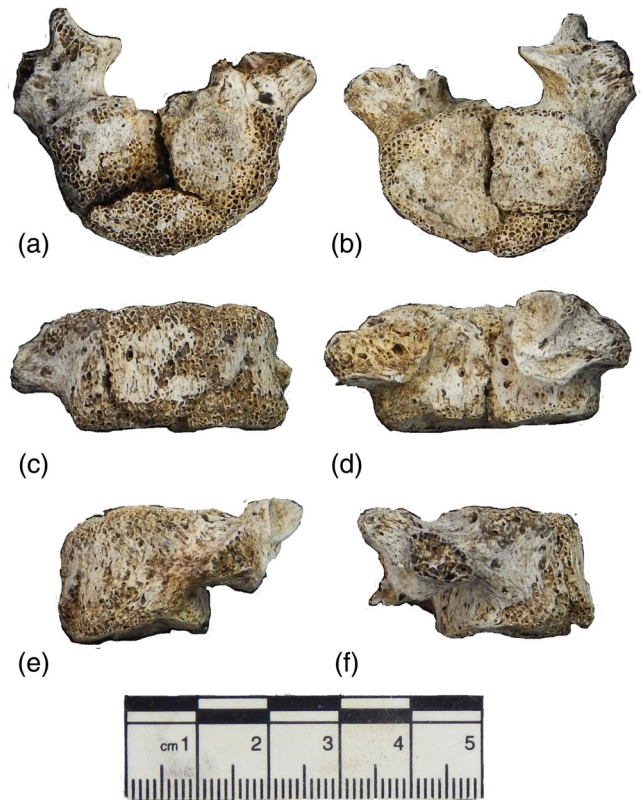
FIGURE 8 Fourth lumbar vertebra (L4), U.W. 102a-306. Views are (a) cranial, (b) caudal, (c) ventral, (d) dorsal, (e) left lateral, and (f) right lateral

FIGURE 9 Fifth lumbar vertebra (L5), U.W. 102a-139. Views are (a) cranial, (b) caudal, (c) ventral, (d) dorsal, (e) left lateral, and (f) right lateral

foramen dorsally. Cranially, the vertebral body is undamaged centrally but it is broken along most aspects of the annular apophysis. It is only complete for about 4 mm at its most lateral aspect on the right side, although the dorsal midline approaches completeness. Caudally, the vertebral body is abraded and exposing trabeculae near the dorsal sagittal midline. The annular apophysis is damaged laterally and ventrally and missing entirely on the right lateral side, along with a portion of the vertebral body itself. Otherwise, the annular apophysis is preserved in places ventrally, laterally, dorsally, and dorsolaterally. Preservation is complete enough to record all vertebral body measurements (Table 2). The 3D wedging angle is estimated as 2.9°.
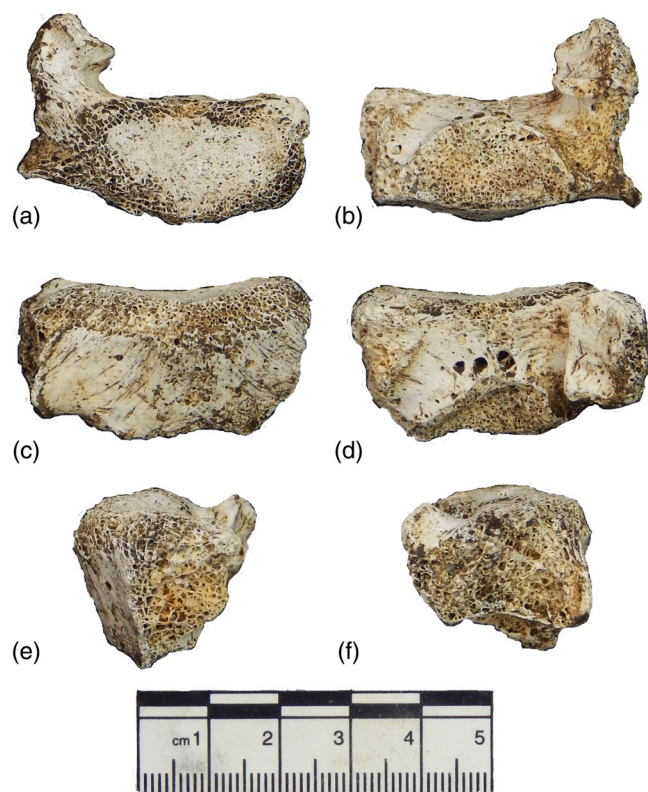
3.4 | Penultimate lumbar vertebra

U.W. 102a-306 is a vertebral body that is wider mediolaterally and craniocaudally shorter than the upper lumbar vertebrae (Figure 8). If a ratio is created between maximum preserved vertebral body width and maximum preserved vertebral body height, U.W. 102a-306 produces a much higher ratio than U.W. 102a-322 (1.37 in U.W. 102a-154B, 1.43 in U.W. 102a-322, 1.83 in U.W. 102a-306, 1.92 in U.W. 102a-139; see below), suggesting there is a gap in the series.

Therefore, a lumbar vertebra (L3) is missing between U.W. 102a-322 and this fossil specimen, the penultimate and fourth lumbar vertebra (Figures 6–8). It preserves the base of the right pedicle, and the base and medial and dorsal extensions of the left pedicle. Pedicle cross-sections are markedly wider mediolaterally and shorter craniocaudally than in the upper lumbar vertebrae. The superior vertebral body is preserved dorsally, but bone is partially abraded laterally on both sides, especially ventrally, exposing trabeculae on the ventral side of the vertebral body. The annular apophysis of the superior vertebral body is only preserved dorsally except cranial to the pedicle, where it is broken, and on each lateral extent of the vertebral body. The inferior vertebral body and annular apophysis are better preserved. A postdepositional pit is present on the caudal surface ventrally near the sagittal midline. This pit is due to taphonomic damage and is not pathological (i.e., Schmorl's node) in nature. The ventral aspect of the inferior vertebral body and annular apophysis are both heavily abraded, exposing trabeculae ventrally. The annular apophysis is chipped but mostly complete on both lateral sides and dorsally. A postdepositional pit is present on the right lateral aspect of the vertebral body between the inferior vertebral body surface and the pedicle base that is also likely the result of taphonomic damage. Preservation only allows for the dorsal height and maximum transverse width of the vertebral body to be measured (Table 2). The 3D wedging angle is estimated at 2.4°.
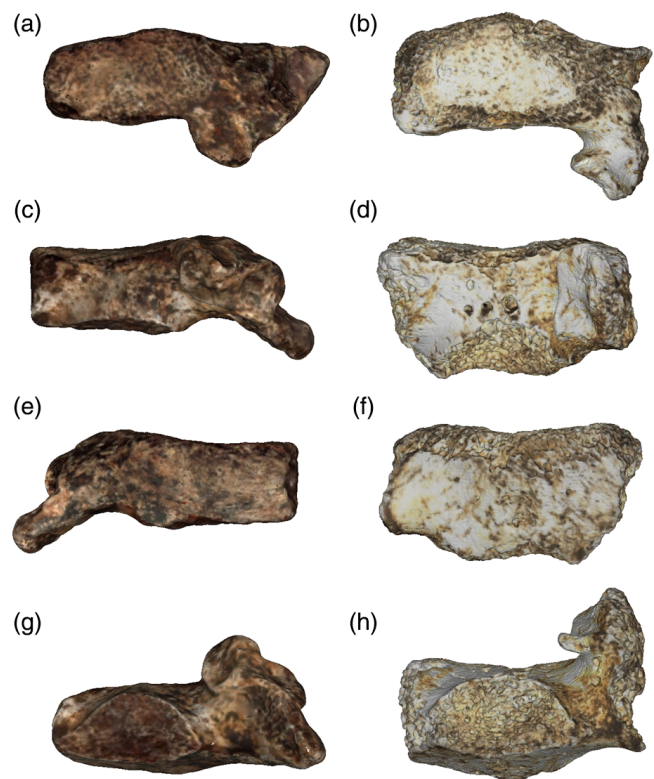
WILLIAMS ET AL.

AMERICAN JOURNAL OF
BIOLOGICAL ANTHROPOLOGY
The Official Journal of the American Association of Biological Anthropologists

WILEY | 7

FIGURE 10 Sacrum, U.W. 102-596. Views are (a) cranial, (b) caudal, (c) ventral, (d) dorsal, (e) left lateral, and (f) right lateral

FIGURE 11 Sacra of *H. naledi* compared. The sacrum from the Dinaledi Chamber (U.W. 101-723) is shown on the left and that from the Lesedi Chamber (U.W. 102-596) is shown on the right. Views are (a–b) cranial, (c–d) dorsal, (e–f) ventral, and (g–h) caudal.
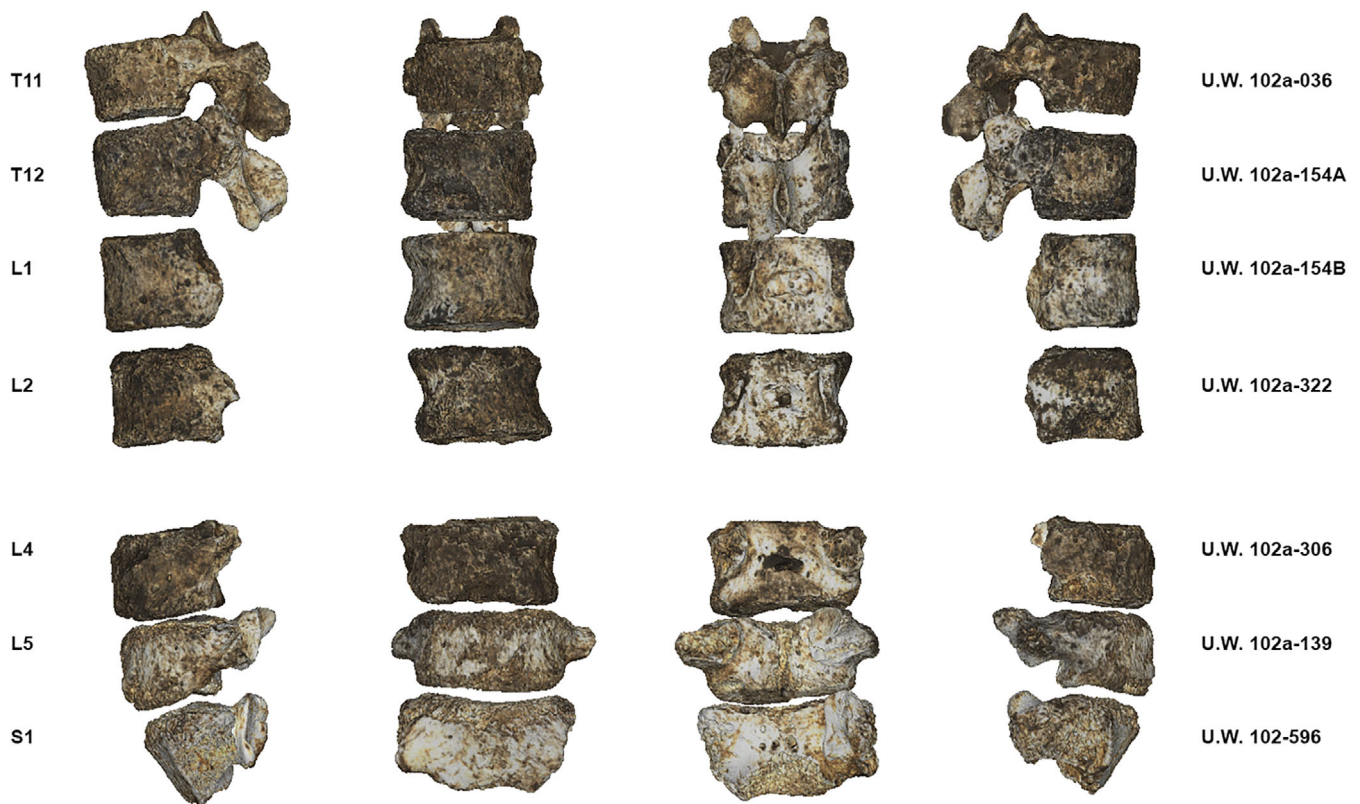
3.5 | Ultimate lumbar vertebra

U.W. 102a-139 is a last lumbar vertebra broken into three main pieces: (i) a fragment consisting of a partial right superior articular process, right pedicle and base of the right transverse process, and right dorsolateral portion of the vertebral body; (ii) a left base of the transverse process and left dorsolateral portion of the vertebral body; (iii) a fragment consisting of the ventral portion of the vertebral body on the sagittal midline and extending laterally approximately 12 mm on both sides (Figure 9). Caudally, the left portion of the vertebral body approaches the midline and joins with the right portion dorsally and in the center of the vertebral body. The left ventral aspect of the inferior vertebral body and annular apophysis is missing, and the annular apophysis is chipped dorsally at midline, on the right lateral side, and on the left dorsolateral aspect of the inferior vertebral body. Cranially and ventrolaterally, the ventral portion of the vertebral body refits with the left portion of the vertebral body. Other areas of contact on the superior vertebral body are missing, exposing trabeculae cranially when the pieces are refit. This continues dorsally such that the superior vertebral body is incomplete at the dorsal midline. The root of the right superior articular process is present inferiorly but is sheared off cranially. Due to its incomplete preservation, only the dorsoventral and maximum transverse width of the inferior vertebral body measurements can be taken on this specimen (Table 2). The 3D wedging angle is estimated at −4.8°.

3.6 | Sacrum

U.W. 102-596 is the upper portion of a sacrum, preserving much of the first sacral body (sacral base), a small (∼5 mm) portion of the medial aspect of the right ala, and most of the right articular process (Figure 10). The sacral body is abraded dorsally, ventrally, and laterally on both sides, precluding exact measurements without estimation. The preserved sacral body measures approximately 33 mm in mediolateral width and 18 mm dorsoventrally at the midline. The sacral body is broken laterally on the left side at its junction with the ala. The articular surface of the right articular process is broken caudally and laterally, but mostly preserved and measures approximately 16 mm craniocaudally and 10 mm mediolaterally. Three basivertebral foramina are present near the sagittal midline of the dorsal vertebral body, within the sacral canal. In terms of overall preservation, this partial sacral fossil is preserved nearly identically to the sacrum from the Dinaledi Chamber (U.W. 101-723; see VanSickle et al., 2018), although U.W. 101-723 preserves more of the ala, forming a more complete upper border of the left anterior sacral foramen than U.W. 102-596 (Figure 11). The Lesedi fossil, however, preserves more of the right superior articular process, whereas the Dinaledi specimen preserves only its base, and the articular surface is sheared off. Despite their similarity in preserved morphology, U.W. 102-596 is substantially larger than

			U.W. 102a-036
T11			
T12			U.W. 102a-154A
L1			U.W. 102a-154B
L2			U.W. 102a-322
L4			U.W. 102a-306
L5			U.W. 102a-139
S1			U.W. 102-596

FIGURE 12 The Lesedi Chamber (U.W. 102) thoracolumbar vertebrae and sacrum. The thoracic and lumbar vertebrae are directly associated with the other LES1 material (102a), whereas the sacrum was recovered from a nearby location (see Figure 1). We propose here the sacrum also belongs to the adult, presumed male individual, LES1 ("Neo"). Views are (right to left): Left lateral, ventral, dorsal, right lateral.

4 | DISCUSSION

The *H. naledi* lumbar vertebrae from the Lesedi Chamber represent the remains of a single, adult individual. The first, second, penultimate, and ultimate lumbar vertebrae (L1, L2, L4, and L5) are preserved. The middle lumbar vertebra (L3) is not present. The lumbar series is part of single vertebral column preceded by three superjacent lower thoracic vertebrae (Hawks et al., 2017) and followed by the subjacent first sacral element (U.W. 102-596) (Figure 12). The lower thoracic vertebrae from the Lesedi Chamber are similar in morphology but larger in size and more robust than those from the Dinaledi Chamber (Berger et al., 2015; Williams et al., 2017). Likewise, U.W. 102-596 preserves nearly identical morphology as the sacrum from Dinaledi (U.W. 101-723; VanSickle et al., 2018) but it is from a slightly larger individual (Figure 11).

To quantify vertebral body wedging angles from the somewhat incomplete Lesedi lumbar vertebrae, we developed a 3D method that does not rely on the preservation of midline structures, as the traditional, linear approach of collecting three measurements based on four landmarks has limited utility in fossil, archeological, or otherwise

U.W. 101-723, matching A.L. 288-1 in approximate size of preserved features.

damaged remains. Only U.W. 102a-154B, the L1 vertebra, preserves the three measurements necessary for calculating the wedging angle using the traditional method, whereas the other lumbar vertebrae from the Lesedi Chamber are missing one or more measurements (Table 2). The 3D wedging angle method we introduce uses a best-fit plane algorithm on 3D surface models. We compare the linear measurement and 3D plane methods in a large sample of modern humans and find them to produce very similar results. The two wedging estimates are significantly and highly ($r^2 = 0.978$) correlated with each other. We are therefore confident that the 3D plane method can be applied to material missing one or more of the midline vertebral body landmarks. Additionally, the high correlation between methods indicates that they can be pooled in future comparisons.

Because the 3D plane method does not rely on the ventral and dorsal midline measurements exclusively, it can be used in cases of broken or otherwise damaged midline structures. The 3D method still requires that most of the vertebral body is present, and if large portions are missing ventrally, dorsally, or laterally, it will not produce an accurate estimate. However, in the case of the *H. naledi* lumbar vertebrae from the Lesedi Chamber, which are increasingly damaged from L1 to L5, the 3D wedging angle method effectively generates wedging angles that the traditional linear wedging angle method cannot. U.W. 102a-154B is the exception as it does preserve all four landmarks required for the linear method. The two methods produce

WILLIAMS ET AL.

AMERICAN JOURNAL OF
BIOLOGICAL ANTHROPOLOGY
The Official Journal of the American Association of Biological Anthropologists

WILEY | 9

nearly identical results for this fossil vertebra (3.8° for the calculated wedging angle and 3.7° for the 3D method).

Using the 3D best-fit plane method, the *H. naledi* individual from the Lesedi Chamber (LES1 "Neo") yields lumbar vertebral body wedging angles consistent with our modern human sample. Other available fossil hominin specimens, including australopiths and Neandertals, similarly fall within the range of preindustrial modern human variation (cf. Whitcome et al., 2007; Williams et al., 2022). This method is useful on vertebral bodies lacking midline measurements, either through damage, pathology, or natural aspects of morphology, but its utility on partial vertebral bodies is more limited, with some states of preservation preventing its use. The fossil lumbar vertebra A.L. 444-7 (male *A. afarensis*) (Ward et al., 2012), for example, preserves too little of the inferior vertebral body surface to estimate the wedging angle accurately. Refinements of the method may permit its estimation, along with that of other insufficiently preserved vertebral bodies, but ultimately adequate preservation or reconstruction is necessary. Overall, however, we recommend using this method on archeological and paleoanthropological material insofar as estimating vertebral body wedging is a useful endeavor.

AUTHOR CONTRIBUTIONS

Scott A. Williams: Conceptualization (lead); data curation (lead); formal analysis (lead); funding acquisition (lead); investigation (lead); methodology (lead); resources (equal); writing – original draft (lead); writing – review and editing (equal). **Iris Zeng:** Conceptualization (equal); data curation (equal); formal analysis (equal); investigation (equal); methodology (equal); writing – review and editing (equal). **Jordan S. Guerra:** Conceptualization (supporting); formal analysis (supporting); investigation (supporting); methodology (supporting); writing – review and editing (supporting). **Shahed Nalla:** Conceptualization (supporting); investigation (supporting); writing – review and editing (equal). **Marina C. Elliott:** Conceptualization (supporting); data curation (equal); funding acquisition (supporting); investigation (equal); project administration (supporting); resources (lead); writing – review and editing (equal). **John Hawks:** Conceptualization (supporting); investigation (supporting); project administration (equal); resources (supporting); writing – review and editing (supporting). **Lee R. Berger:** Conceptualization (equal); data curation (supporting); funding acquisition (supporting); investigation (equal); project administration (equal); resources (equal); writing – review and editing (supporting). **Marc R. Meyer:** Conceptualization (supporting); data curation (equal); formal analysis (supporting); investigation (supporting); methodology (supporting); writing – review and editing (equal).

ACKNOWLEDGMENTS

FUNDING INFORMATION

CONFLICT OF INTEREST

The authors declare that there are no conflicts of interest.

DATA AVAILABILITY STATEMENT

The data that support the findings of this study are available in Tables 1 and 2, and in Supplementary Material 1. 3D models of the *Homo naledi* vertebrae are available on MorphoSource.org. 3D models of human material are not publicly available due to ethical restrictions; however, interested researchers can contact the corresponding author and staff at the institutions acknowledged above where the human remains reside for potential access. In most cases, 3D data access is at the discretion of the museum and other associated entities.

HUMAN REMAINS

The global human sample included in this study consists of human skeletal remains discovered in archeological contexts in the late 19th and early 20th centuries. Individuals were frequently listed by geographical area, and in some museums by population, but the latter are approximations at best and may not accurately reflect ancestry. To our knowledge, none of the individuals included are being sought for repatriation by descendant groups. The lead author signed ethical agreements at most museums to not share 3D data or other images of the human remains without explicit permission of the museum. The lead author will cooperate with any policies enacted by those museums moving forward. All authors herewith acknowledge with deserved honor and respect the inherent scientific contribution from any individual or individuals or persons representing communities or groups of humanity who have knowingly or unknowingly, intentionally or unintentionally, and implicitly or explicitly become part of the researched skeletal collections. It is with unreserved humility and respect that any descendants of the researched individuals are also similarly honored and acknowledged for their contributions.

ORCID

Scott A. Williams https://orcid.org/0000-0001-7860-8962
Shahed Nalla https://orcid.org/0000-0002-0957-1067
John Hawks https://orcid.org/0000-0003-3187-3755

10 | WILEY─AMERICAN JOURNAL OF BIOLOGICAL ANTHROPOLOGY
The Official Journal of the American Association of Biological Anthropologists

WILLIAMS ET AL.

Lee R. Berger 🄳 https://orcid.org/0000-0002-0367-7629

Marc R. Meyer 🄳 https://orcid.org/0000-0002-3938-0173

REFERENCES

Been, E., Gómez-Olivencia, A., & Kramer, P. A. (2012). Lumbar lordosis of extinct hominins. *American Journal of Physical Anthropology, 147,* 64–77. https://doi.org/10.1002/ajpa.21633

Been, E., & Kalichman, L. (2014). Lumbar lordosis. *The Spine Journal, 14,* 87–97. https://doi.org/10.1016/j.spinee.2013.07.464

Berger, L. R., Hawks, J., de Ruiter, D. J., Churchill, S. E., Schmid, P., Delezene, L. K., Kivell, T. L., Garvin, H. M., Williams, S. A., DeSilva, J. M., Skinner, M. M., Musiba, C. M., Cameron, N., Holliday, T. W., Harcourt-Smith, W., Ackermann, R. R., Bastir, M., Bogin, B., Bolter, D., … Zipfel, B. (2015). *Homo naledi,* a new species of the genus *Homo* from the Dinaledi chamber, South Africa. *eLife, 4,* e09560. https://doi.org/10.7554/eLife.09560

Bräuer, G. (1988). Osteometrie. In R. Knussmann (Ed.), *Anthropologie. Handbuch der vergleichenden Biologie des Menschen* (pp. 160–232). Gustav Fischer Verlag.

DiGiovanni, B. F., Scoles, P. V., & Latimer, B. M. (1989). Anterior extension of the thoracic vertebral bodies in Scheuermann's kyphosis: An anatomic study. *Spine, 14,* 712–716.

Hammer, Ø., Harper, D. A., & Ryan, P. (2001). Paleontological statistics software package for education and data analysis. *Paleontologia Electronica, 4,* 1–9.

Hawks, J., Elliott, M., Schmid, P., Churchill, S. E., de Ruiter, D. J., Roberts, E. M., Hilbert-Wolf, H., Garvin, H. M., Williams, S. A., Delezene, L. K., Feuerriegel, E. M., Randolph-Quinney, P., Kivell, T. L., Laird, M. F., Tawane, G., DeSilva, J. M., Bailey, S. E., Brophy, J. K., Meyer, M. R., … Berger, L. R. (2017). New fossil remains of *Homo naledi* from the Lesedi chamber, South Africa. *eLife, 6,* e24232. https://doi.org/10.7554/eLife.24232

Latimer, B., & Ward, C. V. (1993). The thoracic and lumbar vertebrae. In A. Walker & R. Leakey (Eds.), *The nariokotome Homo erectus skeleton* (pp. 266–293). Harvard University Press.

Pickering, T. R., Heaton, J. L., Clarke, R., & Stratford, D. (2019). Hominin vertebrae and upper limb bone fossils from Sterkfontein Caves, South Africa (1998–2003 excavations). *American Journal of Physical Anthropology, 168,* 459–480. https://doi.org/10.1002/ajpa.23758

Smith, R. J. (1984). Allometric scaling in comparative biology: Problems of concept and method. *American Journal of Physiology, 246,* R152–R160. https://doi.org/10.1152/ajpregu.1984.246.2.R152

VanSickle, C., Cofran, Z., García-Martínez, D., Williams, S. A., Churchill, S. E., Berger, L. R., & Hawks, J. (2018). *Homo naledi* pelvic remains from the Dinaledi Chamber, South Africa. *Journal of Human Evolution, 125,* 122–136. https://doi.org/10.1016/j.jhevol.2017.10.001

Ward, C. V., Kimbel, W. H., Harmon, E. H., & Johanson, D. C. (2012). New postcranial fossils of *Australopithecus afarensis* from Hadar, Ethiopia (1990–2007). *Journal of Human Evolution, 63,* 1–51. https://doi.org/10.1016/j.jhevol.2011.11.012

Ward, C. V., Rosenman, B., Latimer, B., & Nalla, S. (2020). Thoracolumbar vertebrae and ribs. In B. Zipfel, B. G. Richmond, & C. V. Ward (Eds.), *Hominin postcranial remains from Sterkfontein, South Africa, 1936–1995* (p. 144). Oxford University Press. https://doi.org/10.1093/oso/9780197507667.003.0010

Whitcome, K. K., Shapiro, L. J., & Lieberman, D. E. (2007). Fetal load and the evolution of lumbar lordosis in bipedal hominins. *Nature, 450,* 1075–1078. https://doi.org/10.1038/nature06342

Williams, S. A., Garcia-Martinez, D., Bastir, M., Meyer, M. R., Nalla, S., Hawks, J., Schmid, P., Churchill, S. E., & Berger, L. R. (2017). The vertebrae and ribs of *Homo naledi. Journal of Human Evolution, 104,* 136–154. https://doi.org/10.1016/j.jhevol.2016.11.003

Williams, S. A., Ostrofsky, K. R., Frater, N., Churchill, S. E., Schmid, P., & Berger, L. R. (2013). The vertebral column of *Australopithecus sediba. Science, 340,* 1232996. https://doi.org/10.1126/science.123299

Williams, S. A., Prang, T. C., Meyer, M. R., Nalley, T. K., Van Der Merwe, R., Yelverton, C., García-Martínez, D., Russo, G. A., Ostrofsky, K. R., Spear, J. K., Eyre, J., Grabowski, M., Nalla, S., Bastir, M., Schmid, P., Churchill, S. E., & Berger, L. R. (2021). New fossils of *Australopithecus sediba* reveal a nearly complete lower back. *eLife, 10,* e70447. https://doi.org/10.7554/eLife.70447

Williams, S. A., Zeng, I., Paton, G. J., Yelverton, C., Dunham, C., Ostrofsky, K. R., Shukman, S., Avilez, M. V., Eyre, J., Loewen, T., Prang, T. C., & Meyer, M. R. (2022). Inferring lumbar lordosis in Neandertals and other hominins. *PNAS Nexus, 1,* pgab005. https://doi.org/10.1093/pnasnexus/pgab005

Zlolinski, S. L., Torres-Tamayo, N., García-Martínez, D., Blanco-Pérez, E., Mata-Escolano, F., Barash, A., Nalla, S., Martelli, S., Sanchis-Gimeno, J. A., & Bastir, M. (2019). 3D geometric morphometric analysis of variation in the human lumbar spine. *American Journal of Physical Anthropology, 170,* 361–372. https://doi.org/10.1002/ajpa.23918

SUPPORTING INFORMATION

Additional supporting information can be found online in the Supporting Information section at the end of this article.